GEOPHYSICS, VOL. 67, NO. 5 (SEPTEMBER-OCTOBER 2002); P. 1564–1574, 12 FIGS., 2 TABLES.
10.1190/1.1512802

Multicomponent stacking-velocity tomography for transversely isotropic media

Vladimir Grechka*, Andres Pech‡, and Ilya Tsvankin‡

ABSTRACT

Accurate estimation of the velocity field is the most difficult step in imaging of seismic data for anisotropic media. Here, the velocity-analysis problem is examined for the most common anisotropic model of sedimentary formations—transverse isotropy (TI) with arbitrary orientation of the symmetry axis. We show that supplementing wide-azimuth reflected PP data with mode-converted (PS) waves yields more stable estimates of the anisotropic coefficients and, in many cases, helps to constrain the model in depth.

An important processing step preceding the inversion is computation of the traveltimes of the pure SS-waves from those of the PP- and PS-waves based on a technique recently developed by Grechka and Tsvankin. This procedure allows us to replace PS-wave moveout, which is generally asymmetric with respect to zero offset, with the symmetric (hyperbolic on short spreads) moveout of the pure SS reflections. Then, generalizing the algorithm previously suggested for PP data, we develop a joint tomographic inversion of the normal-moveout (NMO) ellipses and zero-offset traveltimes of PP- and SS-waves.

Application of the method to wide-azimuth PP and PS reflections from a dipping interface beneath a homogeneous TI layer shows that for a range of reflector dips and tilt angles of the symmetry axis, it is possible to build the anisotropic velocity field in the depth domain. We also extend our inversion procedure to layered TI media with curved interfaces and study its stability in the presence of noise and heterogeneity.

INTRODUCTION

A number of case studies involving multicomponent land and offshore data demonstrated that mode (P-to-S) conversions can supplement or even replace pure-mode reflections in such applications as imaging beneath gas clouds (e.g., Granli et al., 1999; Thomsen, 1999) and characterization of fractured reservoirs (e.g., Pérez et al., 1999). Processing of PS-waves, however, is complicated by the strong influence of seismic anisotropy on their signatures. For example, the velocity anisotropy of SV- and PSV-waves in transversely isotropic (TI) media is mostly controlled by the coefficient

$$\sigma \equiv \left(\frac{V_{P0}}{V_{S0}}\right)^2 (\epsilon - \delta), \tag{1}$$

which is typically much larger than the Thomsen (1986) parameters ϵ and δ governing P-wave data (V_{P0} and V_{S0} are the vertical P- and S-wave velocities, respectively). Mis-ties between PP and PS sections routinely produced by conventional isotropic imaging methods (e.g., Nolte et al., 1999) indicate the need for joint anisotropic velocity analysis of PP and PS reflection events.

As shown by Tsvankin and Grechka (2000a,b) for transversely isotropic media with a vertical symmetry axis (VTI), wide-azimuth reflection traveltimes of PP- and PSV-waves from a single mildly dipping reflector are sufficient for estimating all relevant parameters (V_{P0}, V_{S0}, ϵ, and δ). However, if the reflector is horizontal, the joint inversion of PP and PSV moveout data is nonunique, even if uncommonly long offsets are available (Grechka and Tsvankin, 2003a). It should be emphasized that the vertical velocity and reflector depth are difficult to determine using PP moveout alone. Le Stunff et al. (2001) and Grechka et al. (2000a,b) showed that depth-domain velocity analysis of PP reflections in VTI media is feasible for only a limited subset of models with dipping or curved intermediate boundaries.

Here we extend our previous results on the inversion of PP and PS data (Grechka et al., 2000a,b; Tsvankin and Grechka,

Manuscript received by the Editor May 29, 2001; revised manuscript received December 26, 2001.
*Formerly Colorado School of Mines, Center for Wave Phenomena, Golden, Colorado 80401-1887; presently Shell International Exploration and Production Inc., Bellaire Technology Center, 3737 Bellaire Blvd., Houston, Texas 77001-0481.
‡Colorado School of Mines, Center for Wave Phenomena, Department of Geophysics, Golden, Colorado 80401-1887. E-mail: apech@dix.mines.edu; ilya@dix.mines.edu.

2000a,b) by introducing the methodology of anisotropic multicomponent stacking-velocity tomography and applying it to TI media with an arbitrary tilt of the symmetry axis. Rather than working with PS data directly, we combine them with PP data to obtain the traveltimes of the pure SS (SV or SH for TI media) reflections from the same interface using the algorithm of Grechka and Tsvankin (2002b). The computation of SS traveltimes is entirely data-driven and does not require exact knowledge of the velocity model. This procedure makes it possible to avoid inherent problems of PS-wave velocity analysis caused by the asymmetry of PS moveout with respect to zero offset on CMP (common-midpoint) and CCP (common-conversion-point) gathers, conversion-point dispersal, and polarity reversals.

In contrast to the more complicated moveout of mode conversions, reflection traveltime of pure SS-waves on CMP gathers is symmetric with respect to zero offset and, for moderate offset-to-depth ratios, can be described by the NMO ellipse (Grechka and Tsvankin, 1998). Hence, the theory of the NMO ellipses and NMO-velocity surfaces (Grechka et al., 1999; Grechka and Tsvankin, 2002a) is directly applicable to SS-wave moveout. In particular, Grechka and Tsvankin (2002a) showed that pure-mode NMO ellipses in heterogeneous arbitrary anisotropic media can be built in a computationally efficient way by tracing just one (zero-offset) ray for each reflection event. This modeling technique was used by Grechka et al. (2000a,b) to develop tomographic-style inversion of PP-wave NMO ellipses in VTI media composed of homogeneous layers separated by planar or curved interfaces.

The methodology of Grechka et al. (2000a,b) is generalized here for the combination of conventional-spread PP and SS data. The tomographic algorithm operates with the NMO ellipses, zero-offset traveltimes, and reflection slopes of PP-waves and SS-waves (the SS traveltimes are supposed to be obtained from the PP and PS data). We examine a wide range of homogeneous TI models with a tilted symmetry axis (including horizontal transverse isotropy, or HTI) and establish the conditions needed for stable parameter estimation. The proposed method is then applied to layered TI models to estimate the interval medium parameters and the shapes of interfaces from multicomponent reflection data.

METHODOLOGY OF STACKING-VELOCITY TOMOGRAPHY

The goal of the tomographic algorithm introduced here is to estimate the anisotropic subsurface model using wide-azimuth measurements of stacking (moveout) velocities of PP- and SS-waves on moderate-length CMP spreads (i.e., spreads close to the reflector depth). Therefore, this approach can be classified as anisotropic multicomponent stacking-velocity tomography.

Although limiting the input data to stacking velocities excludes the far-offset information from analysis, our algorithm is much more computationally efficient than conventional reflection tomography (e.g., Le Stunff and Grenié, 1998). Indeed, azimuthally varying moveout velocity, described by the NMO ellipse, can be computed by tracing only one zero-offset ray per CMP and per reflector (Grechka and Tsvankin, 2002a; Grechka et al., 2000a,b). A more detailed comparison of stacking-velocity tomography with the conventional method is given in the Discussion and Conclusions section.

We implemented the multicomponent tomographic procedure for TI media composed of homogeneous layers separated by plane or smooth curved interfaces. The algorithm includes the following main steps:

1) Picking PP and PS traveltimes from prestack 3-D data volumes and identifying the PP and PS events reflected from the same interfaces. In general, both split converted waves (PS_1 and PS_2) can be used.
2) Computing the traveltimes of the pure SS (S_1S_1 and S_2S_2) reflections from PP and PS data using the method of Grechka and Tsvankin (2002b).
3) Performing azimuthal velocity analysis to obtain the NMO ellipses of the PP- and SS-waves (Grechka and Tsvankin, 1999a).
4) Inverting the NMO ellipses, zero-offset traveltimes, and reflection slopes for the interval anisotropic parameters by extending the approach of Grechka et al. (2000a,b) to multicomponent data.

The data vector used in the inversion for an N-layered TI medium is given by

$$\mathbf{d}(Q, \mathbf{Y}, n) \equiv \{\tau_Q(\mathbf{Y}, n), \mathbf{p}_Q(\mathbf{Y}, n), \mathbf{W}_Q(\mathbf{Y}, n)\}, \qquad (2)$$

where $Q =$ PP or SS is the mode type (only SV SV-waves are included in the algorithm discussed here), $\mathbf{Y} = [Y_1, Y_2]$ is the CMP location, $n = 1, 2, \ldots, N$ is the reflector number, τ is the zero-offset traveltime, $\mathbf{p}$ is the reflection slope on zero-offset time sections, and $\mathbf{W}$ is the 2×2 matrix (Grechka and Tsvankin, 1998) describing the NMO ellipse.

Our goal is to find the model vector $\mathbf{m}$ which contains the interval medium parameters and the coefficients of the polynomials used to describe the model interfaces. For TI media with an unknown tilt of the symmetry axis, the inversion of PP- and SV SV-waves can be used to estimate six interval parameters: the symmetry-direction P- and S-wave velocities V_{P0} and V_{S0}, anisotropic coefficients ϵ and δ, and two angles responsible for the symmetry-axis orientation.

In general, the parameter-estimation algorithm is organized in the same way as that introduced for PP-waves by Grechka et al. (2000a,b). For a given set of trial interval anisotropic parameters, the zero-offset traveltimes τ_Q and the reflection slopes $\mathbf{p}_Q$ are used to compute the one-way zero-offset rays for all reflection events. Then the interfaces for the trial model are reconstructed by fitting 2-D polynomials to the termination points of the zero-offset rays, which allows us to compute the NMO ellipses. Finally, the interval parameters are obtained by minimizing the following objective function:

$$\mathcal{F}(\mathbf{m}) \equiv \sum_{Q,\mathbf{Y},n} \left\| \mathbf{W}_Q^{\text{calc}}(\mathbf{Y}, n, \mathbf{m}) - \mathbf{W}_Q^{\text{meas}}(\mathbf{Y}, n) \right\|. \qquad (3)$$

The norms in the function (3) contain the differences between the computed and measured NMO ellipses $\mathbf{W}$ for all modes and all reflectors at each CMP location.

INVERSION OF PP AND SS DATA FOR A HOMOGENEOUS TI MEDIUM

Consider the model of a single homogeneous TI layer with a planar lower boundary (horizontal or dipping) and arbitrary orientation of the symmetry axis. The problem addressed here is whether wide-azimuth reflection traveltimes of PP- and

SS(SV SV)-waves (SS traveltimes are computed from PP and PS data) can be inverted for the symmetry-direction velocities V_{P0} and V_{S0}, the parameters ϵ and δ, and the axis orientation.

It is convenient to study the feasibility of parameter estimation by applying the weak-anisotropy approximation to the NMO ellipses and zero-offset traveltimes. The analysis has to be performed for P-waves only, because any kinematic signature of SV-waves for weak transverse isotropy can be obtained from the corresponding P-wave signature by making the following substitutions: $V_{P0} \to V_{S0}$, $\delta \to \sigma$, and $\epsilon \to 0$ (Tsvankin, 2001; see Table 1 below). A similar substitution rule for SH-waves is $V_{P0} \to V_{S0}, \delta \to \gamma$, and $\epsilon \to \gamma$. SH-wave anisotropy, however, is elliptical, and most kinematic signatures can be obtained in closed form without applying the weak-anisotropy approximation.

VTI layer

The substitution rules for different modes hold (in the weak-anisotropy limit) for the processing parameters as well. Alkhalifah and Tsvankin (1995) showed that P-wave time processing in VTI media with a laterally homogeneous overburden above the target reflector is governed by the zero-dip P-wave NMO velocity

$$V^2_{\mathrm{nmo},P} = V^2_{P0}(1+2\delta) \tag{4}$$

and the anellipticity coefficient

$$\eta \equiv \frac{\epsilon-\delta}{1+2\delta}. \tag{5}$$

Note that this result is valid for any strength of velocity anisotropy. Time processing of SV-waves for weakly anisotropic VTI media is then controlled by the zero-dip SV-wave NMO velocity

$$V^2_{\mathrm{nmo},SV} = V^2_{S0}(1+2\sigma) \tag{6}$$

and the parameter $[-\sigma/(1+2\sigma)]$ that plays the role of η [σ was introduced in equation (1)]. Time processing of elliptically anisotropic SH-waves requires just the NMO velocity

$$V^2_{\mathrm{nmo},SH} = V^2_{S0}(1+2\gamma) \tag{7}$$

because the quantity corresponding to η goes to zero. This well-known result implies that isotropic time-processing algorithms are entirely valid for elliptical anisotropy (Dellinger and Muir, 1988; Alkhalifah and Tsvankin, 1995).

Suppose the data include multiazimuth (3-D) traveltimes of PP- and PSV-reflections from a planar dipping interface below a homogeneous VTI layer. Without losing generality, the dip plane of the reflector is assumed to coincide with the coordinate plane $[x_1, x_3]$ (i.e., the x_1-axis points in the dip direction).

Table 1. Correspondence between the parameters responsible for the kinematic signatures of P-, SV-, and SH-waves in weakly anisotropic TI media.

Parameter	P	SV	SH
Kinematic	V_{P0}	V_{S0}	V_{S0}
	ϵ	0	γ
	δ	σ	γ
Time Processing (VTI)	$V_{\mathrm{nmo},P}$	$V_{\mathrm{nmo},SV}$	$V_{\mathrm{nmo},SH}$
	η	$-\sigma$	0

Applying the methodology of Grechka and Tsvankin (2002b), we compute the traveltimes of the pure SS (SV SV) reflections and use azimuthal moveout analysis (Grechka and Tsvankin, 1999a) to obtain the NMO ellipses of both PP- and SS-waves.

Since the model is symmetric with respect to the dip plane, the axes of the NMO ellipses have to be aligned with the dip and strike directions (Grechka and Tsvankin, 1998). The linearized approximations for the semiaxes of the PP-wave NMO ellipse are given by (Alkhalifah and Tsvankin, 1995; Grechka and Tsvankin, 1998)

$$V^2_{\mathrm{nmo},P,\mathrm{dip}}(p_{P,1}) = \frac{V^2_{\mathrm{nmo},P}}{1-y_P}\left[1+\frac{2\eta y_P}{1-y_P}\left(6-9y_P+4y_P^2\right)\right] \tag{8}$$

and

$$V^2_{\mathrm{nmo},P,\mathrm{strike}}(p_{P,1}) = V^2_{\mathrm{nmo},P}[1+2\eta y_P(2-y_P)], \tag{9}$$

where

$$y_P \equiv p^2_{P,1}V^2_{\mathrm{nmo},P},$$

$p_{P,1}$ is the horizontal slowness component of the PP-wave zero-offset ray (or the dip component of the reflection slope), and the strike component $p_{P,2}=0$. Equations (8) and (9) can be inverted for the zero-dip NMO velocity $V_{\mathrm{nmo},P}$ and the anisotropic coefficient η if the reflector dip (expressed through the slope $p_{P,1}$) is not too small. The inversion of the PP-wave NMO ellipse using the exact equations is discussed by Grechka and Tsvankin (1998), who find that the dip should exceed 25° to ensure stable estimation of η.

The weak-anisotropy approximations for the dip and strike components of the SV-wave NMO velocity can be obtained directly from equations (8) and (9) using the conversion rule from Table 1:

$$V^2_{\mathrm{nmo},SV,\mathrm{dip}}(p_{SV,1}) = \frac{V^2_{\mathrm{nmo},SV}}{1-y_{SV}}\left[1-\frac{2\sigma y_{SV}}{1-y_{SV}} \times \left(6-9y_{SV}+4y_{SV}^2\right)\right], \tag{10}$$

$$V^2_{\mathrm{nmo},SV,\mathrm{strike}}(p_{SV,1}) = V^2_{\mathrm{nmo},SV}[1-2\sigma y_{SV}(2-y_{SV})]. \tag{11}$$

Here

$$y_{SV} \equiv p^2_{SV,1}V^2_{\mathrm{nmo},SV},$$

$p_{SV,1}$ is the horizontal slowness component of the SS-wave zero-offset ray, and the strike component $p_{SV,2}=0$.

Similarly to the parameter estimation for PP-waves described above, equations (10) and (11) can be inverted for $V_{\mathrm{nmo},SV}$ and σ. Furthermore, substituting $V_{\mathrm{nmo},SV}$ and σ into equation (6) yields the shear-wave vertical velocity V_{S0}. Then the zero-offset traveltime and the reflection slope of the SS reflection can be used to reconstruct the depth and dip of the reflector.

Next, we demonstrate that adding this information to the traveltimes of PP-waves is sufficient for estimating the vertical velocity V_{P0} and the anisotropic coefficients ϵ and δ. The equation of the planar reflecting interface defined by the coordinate vector $\mathbf{x}$ can be written in the form

$$\mathbf{n}\cdot(\mathbf{x}-\mathbf{r}_P)=0, \tag{12}$$

where $\mathbf{n}$ is a unit vector normal to the reflector and $\mathbf{r}_P$ defines the PP-wave zero-offset reflection point. Similarly, for the zero-offset SS ray reflected from the point $\mathbf{r}_{SV}$, we have

$$\mathbf{n}\cdot(\mathbf{x}-\mathbf{r}_{SV})=0. \tag{13}$$

Combining equations (12) and (13) yields

$$\mathbf{n}\cdot\mathbf{r}_P=\mathbf{n}\cdot\mathbf{r}_{SV}. \tag{14}$$

The vector $\mathbf{n}$ can be replaced in equation (14) by the normalized (so that the magnitude is equal to unity) slowness vectors of the zero-offset PP and SS rays because the slowness (or phase-velocity) vectors of pure-mode reflections at zero offset are orthogonal to the reflector. Also, the vectors $\mathbf{r}_P$ and $\mathbf{r}_{SV}$ can be expressed through the group-velocity vectors of the PP- and SS-waves by putting the origin of the coordinate system at the CMP location. Then linearization of equation (14) in the anisotropic parameters leads to

$$\begin{aligned}&\tau_P V_{\mathrm{nmo},P}\left[1-\delta\left(1-p_{P,1}^2V_{\mathrm{nmo},P}^2\right)+\eta p_{P,1}^4V_{\mathrm{nmo},P}^4\right]\\&\quad=\tau_{SV}V_{\mathrm{nmo},SV}\left[1-\sigma\left(1-p_{SV,1}^2V_{\mathrm{nmo},SV}^2+p_{SV,1}^4V_{\mathrm{nmo},SV}^4\right)\right],\end{aligned} \tag{15}$$

where τ_P and τ_{SV} are the zero-offset traveltimes of the PP- and SS-arrivals. Note that the quantities on the left- and right-hand sides of equation (15) comply with the conversion rule in Table 1. The result equivalent to equation (15) can be obtained by using Snell's law for the zero-offset P- and SV-rays instead of equations (12) and (13).

Although the parameters $V_{\mathrm{nmo},P}$, $V_{\mathrm{nmo},SV}$, η, and σ, which can be obtained from the PP- and SS-wave NMO ellipses [equations (8)–(11)], are sufficient to find the vertical velocities V_{P0} and V_{S0} and the coefficients ϵ and δ, the inversion of the PP-wave NMO ellipse for η requires reflector dips of at least 25° (Alkhalifah and Tsvankin, 1995; Grechka and Tsvankin, 1998). The NMO ellipse of the SS-wave is more sensitive to dip than that of the PP-wave because of relatively large values of σ. Supplementing equations (8)–(11) with equation (15) adds another constraint on the anisotropic parameters and helps to obtain an accurate result for dips below 25°. Indeed, the numerical tests below confirm that dips as small as 15° are sufficient for stable estimation of the VTI parameters for this simple model.

Figure 1 illustrates application of our methodology to noise-contaminated wide-azimuth PP and SS (SV SV) traveltimes (the SS traveltimes are supposed to be computed from the PP and PS data) generated for a homogeneous VTI layer with the lower boundary dipping at 15°. We applied nonlinear inversion (the Gauss-Newton method) based on the exact equations for the NMO ellipses, zero-offset traveltimes, and reflection slopes; the objective function is given in equation (3). The dots in Figure 1 mark the estimated VTI parameters for different realizations of the noise added to the input data. The standard deviations in the inverted parameters (2% for V_{P0} and V_{S0}, 0.03 for ϵ, and 0.02 for δ) indicate that the noise does not get amplified by the parameter-estimation procedure, so the inversion is reasonably stable. Note that the estimated values of ϵ and δ cluster near the line of the correct parameter $\eta\approx\epsilon-\delta$ because the difference $\epsilon-\delta$ is well constrained by both PP and SS traveltimes (Tsvankin and Grechka, 2000a).

The only parameter of VTI media that cannot be obtained from P and SV data is γ—the anisotropic coefficient responsible for the elliptical anisotropy of SH-waves. Tsvankin and Grechka (2000b) showed that γ can be determined from converted PSH-waves, which are generated for all azimuthal directions outside the dip plane. The methodology introduced here can be applied to the estimation of γ from the NMO ellipses of the pure SH-wave reflections computed from PP and PSH data. Thus, with the combination of PP-, PSV-, and PSH-wave reflection traveltimes, one can estimate all five VTI parameters and build the anisotropic depth model.

HTI layer

Contreras et al. (1999) studied the inversion of wide-azimuth PP data for HTI media and showed that the symmetry-direction velocity V_{P0}, the coefficients ϵ and δ (or $\epsilon^{(V)}$ and $\delta^{(V)}$; see Tsvankin, 1997), and the azimuth β of the horizontal symmetry axis can be found from the PP-wave NMO ellipses from a horizontal and a dipping reflector. However, the need to use two different dips for each depth interval makes this algorithm difficult to implement in practice. In contrast, our approach is designed to estimate the HTI parameters using the NMO ellipses of PP- and SS(SV SV)-waves from a single reflector that can be either horizontal or dipping. Note that by SV-wave we always mean the mode polarized in the plane formed by the slowness vector and the symmetry axis. If the symmetry axis is horizontal or tilted, this plane is no longer necessarily vertical, but we still prefer to keep the notation commonly used for VTI media.

The inversion for a horizontal HTI layer confirms the results of Tsvankin (1997), who pointed out that the combination of wide-azimuth PP- and SS-wave moveout data is sufficient for estimating the symmetry-direction velocities V_{P0} and V_{S0} and the parameters ϵ and δ. For this model, the velocities V_{P0} and V_{S0} can be found directly from surface data because they are equal to the corresponding NMO velocities measured in the direction orthogonal to the symmetry axis (i.e., in the isotropy plane). Typical results of inverting noise-contaminated PP and SS traveltimes for the parameters of a horizontal HTI layer are shown in Figure 2. In this example, the standard deviations in all

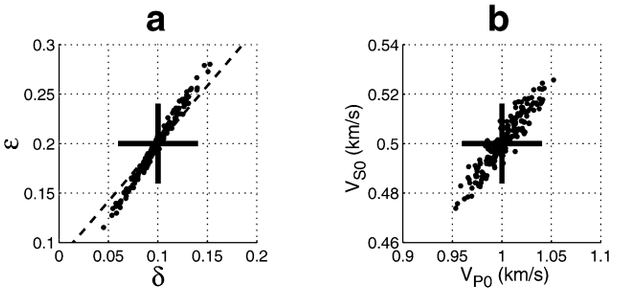

FIG. 1. Results (dots) of the joint inversion of PP and SS (SV SV) data for a single VTI layer above a planar dipping reflector. The correct layer parameters are marked by the crosses; the reflector dip is 15°. The dashed line on plot (a) corresponds to the correct value of η. The data were contaminated by Gaussian noise with the standard deviations equal to 2% for the NMO velocities and 1% for the zero-offset traveltimes and reflection slopes.

estimated parameters, including the azimuth β of the symmetry axis (not shown on the plot), are quite small; the deviation in β is just 0.6°.

To examine the inversion for dipping interfaces, we adapted for SS-waves (see the substitution rule in Table 1) the weak-anisotropy approximations for PP-wave NMO ellipses given by Contreras et al. (1999). These results are similar to the ones discussed in the previous section for VTI media and, therefore, are not given here. Both the theoretical analysis and the inversion based on the exact equations (see Figure 3) prove that the parameter estimation remains stable for the whole range of dips from 0° to 90°.

The dots of the estimated parameter values in Figure 3 form smaller clouds than those in Figure 1, which indicates that the inversion of dipping events for HTI media is more stable compared to that for VTI media. (As discussed above, for a horizontal VTI layer the inversion for V_{P0}, V_{P0}, ϵ, and δ cannot be performed at all.) We also noticed that the inversion algorithm for HTI media converges much more rapidly toward the correct model than it does for VTI media.

TTI layer

The parameter-estimation problem for transverse isotropy with a tilted symmetry axis (TTI media) includes only one additional unknown compared to the HTI case—the tilt ν. This, however, makes the inversion substantially more ill posed than that for HTI media because the pure-mode NMO ellipses are nonlinear functions of ν, even for weak anisotropy. Grechka and Tsvankin (2000) found a nonlinear dependence on the tilt in the weak-anisotropy approximation for the PP-wave NMO ellipse in TTI media, and adaptation of their equations for shear modes using Table 1 leads to the same result for both SV- and SH-waves. Therefore, the misfit (objective) function for the NMO ellipses that has to be minimized in the nonlinear inversion typically has local minima, even for weak anisotropy. The multimodal nature of the misfit function may require several inversions starting from different points in the model space.

The schematic summary of our numerical results in Figure 4 illustrates the influence of the tilt of the symmetry axis and reflector dip on the uniqueness of parameter estimation in TTI media. This plot should not be interpreted in a strict quantitative sense because the criteria we used to identify the areas of unique and nonunique inversion are somewhat loose. In general, the line dividing those areas corresponds to the standard deviations in ϵ and δ of about 0.03 (for the errors in the input data given in the caption of Figure 1). However, the quality of the inversion results also depends on parameters not shown in Figure 4 such as the magnitude of ϵ and δ and the azimuth of the symmetry axis. In particular, the inversion becomes more stable with increasing absolute values of ϵ and δ.

It should be emphasized that in generating Figure 4 we assumed the orientation of the symmetry axis is unknown, even if the model is HTI or VTI. Therefore, the stability of the inversion results for both VTI and HTI is lower than that in the two previous sections on VTI and HTI media where we fixed the tilt of the symmetry axis at the correct value (see Figures 1–3). Still, Figure 4 shows that even if the HTI model is not assumed in advance, it can be accurately reconstructed from reflection data despite some problems caused by the more complicated topology (e.g., multiple local minima) of the objective function.

In contrast, when the tilt of the symmetry axis is small (i.e., the model is close to VTI) and *unknown*, the inversion remains ambiguous for all reflector dips. As the symmetry axis deviates further from the vertical, the inversion becomes more stable (for a fixed dip) and can be performed for an increasingly wide

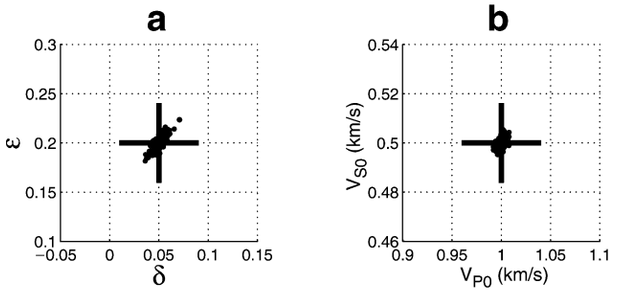

FIG. 2. Results of the inversion (dots) of PP and SS data for a horizontal HTI layer using the exact equations for the NMO ellipses. The data were contaminated by noise with the same standard deviations as those in Figure 1. The correct layer parameters are marked by the crosses. V_{P0} and V_{S0} are the velocities in the symmetry-axis direction.

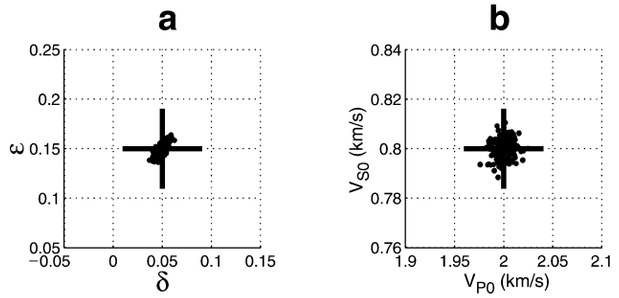

FIG. 3. Same as Figure 2 but for an HTI layer with the lower boundary dipping at 25°. The azimuth of the symmetry axis with respect to the dip plane is $\beta = 40°$; the standard deviation in β is 0.8°.

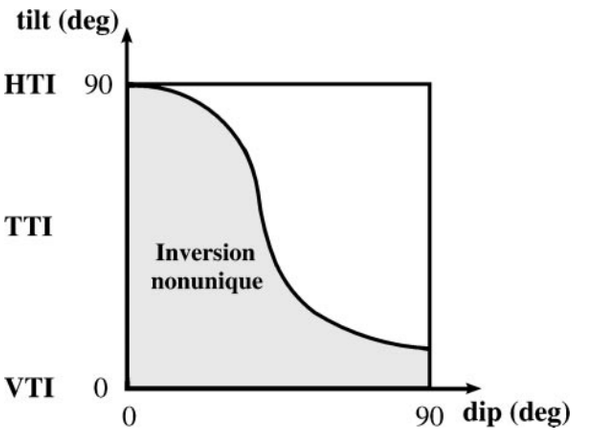

FIG. 4. Uniqueness of depth-domain parameter estimation in TI media for the full range of reflector dips and tilt angles of the symmetry axis. The tilt and azimuth of the symmetry axis were unknown (i.e., they were estimated from the inversion) for all models, including VTI and HTI media.

range of dips (Figure 4). For HTI media (see above) the inversion is feasible even for a horizontal reflector and without a priori knowledge of the tilt.

Figure 5 displays inversion results typical for models located within the area of nonuniqueness in Figure 4 near the area's boundary. As in the previous examples, we inverted the NMO ellipses, zero-offset traveltimes, and reflection slopes of the PP- and SS-waves after contaminating the input data with Gaussian noise. Although the obtained parameters scatter around the correct values, the standard deviations (4% in V_{P0} and V_{S0}, 0.05 in ϵ, 0.04 in δ, 1.5° in β, and 0.8° in ν) indicate a substantial error amplification in the estimation of V_{P0}, V_{S0}, ϵ, and δ.

The stability of the inversion for TTI models may be enhanced by including SH-wave NMO ellipses and zero-offset traveltimes in the input data. The traveltimes of pure SH reflections can be obtained using PSH converted waves generated for source-receiver azimuths outside of the vertical symmetry plane(s) of the model (see the discussion above).

Thus, multicomponent (PP and PS), multiazimuth reflection data can be inverted for the parameters of homogeneous TI media for a range of reflector dips and tilts of the symmetry axis. The highest stability is observed for near-horizontal orientations of the symmetry axis, while for a vertical or tilted symmetry axis the inversion becomes more stable with increasing dip.

PARAMETER ESTIMATION FOR LAYERED TI MEDIA

Here we describe application of the multicomponent tomographic procedure to TI models containing homogeneous layers with arbitrary orientation of the symmetry axis separated by smooth curved interfaces. Suppose the input data include wide-azimuth traveltimes of PP- and PSV-waves reflected from the two interfaces of the VTI model in Figure 6. After computing the traveltimes of the pure SS reflections using the method of Grechka and Tsvankin (2002b), we collect the PP and SS data into CMP gathers for azimuthal velocity analysis. Estimating the PP- and SS-wave NMO ellipses and zero-offset traveltimes at four CMP locations (Figure 6) yields the data vector from equation (2). Then, for each trial model we build the interfaces and compute the objective function (2), which is then minimized using the nonlinear inversion algorithm.

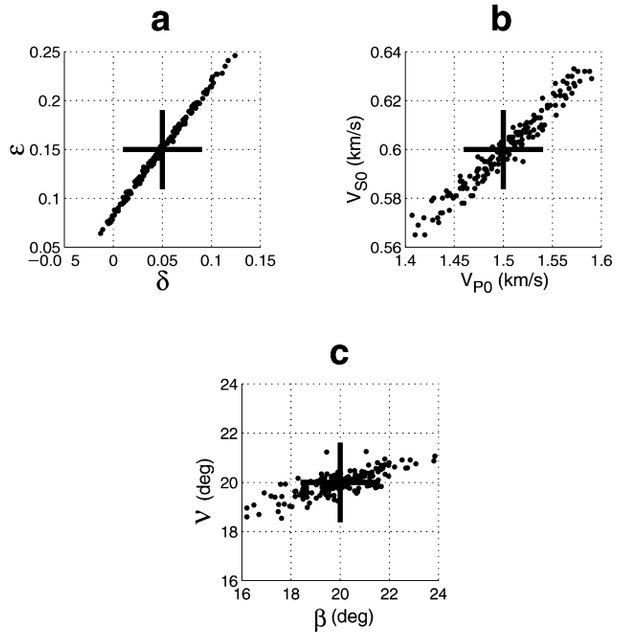

FIG. 5. Results of the inversion (dots) of PP and SS traveltime data for a dipping TTI layer (the dip is 30°; tilt is 20°). The data were contaminated by noise with the same standard deviations as those in Figure 1. The correct layer parameters are marked by the crosses. V_{P0} and V_{S0} are the velocities in the symmetry-axis direction; ν and β are the tilt and azimuth of the symmetry axis, respectively (β is measured with respect to the dip plane).

Numerical examples

The input data from Figure 6 were distorted by Gaussian noise with the standard deviation of 2% for the NMO velocities and 1% for the zero-offset traveltimes and reflection slopes. The inversion results for 100 realizations of the input data in Figure 7 indicate that the noise does not get amplified by the parameter-estimation procedure. The standard deviations in the inverted parameters are about 0.01 for ϵ and δ, and less than 1% for V_{P0} and V_{S0} (not shown).

Note that neither of the interfaces in the model from Figure 6 has steeply dipping segments. In agreement with the results for a single layer, the high sensitivity of the SS-wave NMO ellipse to reflector dip and the addition of the ratio of the zero-offset PP and SS traveltimes [equation (15)] ensures the stability of the joint inversion of wide-azimuth PP and SS data for dips of 15–20°.

Figures 8 and 9 show the tomographic inversion of multicomponent data for a more complicated model that includes VTI,

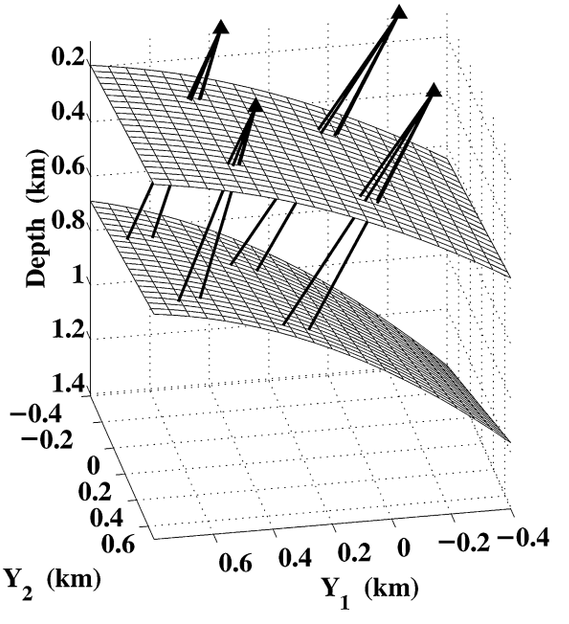

FIG. 6. Zero-offset rays of the PP- and SS(SV SV)-waves recorded at four CMP locations over a model composed of two homogeneous VTI layers. The parameters of the top layer are $V_{P0,1} = 2.0$ km/s, $V_{S0,1} = 0.8$ km/s, $\epsilon_1 = 0.15$, and $\delta_1 = 0.05$. For the bottom layer, $V_{P0,2} = 2.5$ km/s, $V_{S0,2} = 0.9$ km/s, $\epsilon_2 = 0.20$, and $\delta_2 = 0.10$.

HTI, and TTI layers. Despite the larger error bars for deeper horizons, the overall stability of the algorithm is satisfactory. A general increase in errors with depth, caused by the relatively small contribution of the deeper layers to the reflection traveltimes from their lower boundaries, is typical for all kinematic inversion algorithms. Also, although we do not differentiate Dix-type formulae explicitly to obtain the interval anisotropic coefficients, errors in the parameters of the upper layers still propagate into the inversion results for the deeper part of the section.

Influence of errors in the symmetry type

In the examples discussed in the previous section, it was assumed that the type of anisotropy (i.e., anisotropic symmetry) in each layer was known in advance. Since this is not necessarily the case in practice, it is instructive to examine the inversion of error-free data using an intentionally incorrect anisotropic symmetry in one of the layers.

We specified a TI model composed of two VTI layers on top of an HTI layer (Figure 10) with the interval parameters listed in the top row of Table 2. Then the tomographic parameter estimation was performed under the erroneous assumption that the bottom (HTI) layer has VTI symmetry (the second row in Table 2). As expected, the inversion produced seriously distorted values of the symmetry-direction velocities $V_{P0,3}$ and $V_{S0,3}$ and the anisotropic coefficients ϵ_3 and δ_3. It is interesting that the parameters of the two upper layers are also inaccurate because the error in the bottom layer gets distributed throughout the whole model to minimize the objective function (3). Hence, errors can propagate not only downward (accumulate with depth) but also upward, albeit with a substantially smaller amplification.

Another implication of this observation is that it might be preferable to perform tomographic inversion in a layer-stripping mode, starting with estimation of the parameters of

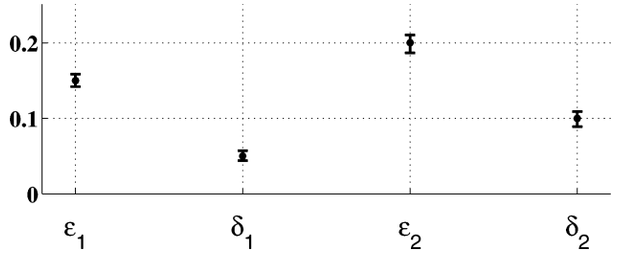

FIG. 7. Results of stacking-velocity tomography for the model in Figure 6. The dots mark the exact values of the anisotropic parameters; the bars correspond to the ± standard deviation in each parameter.

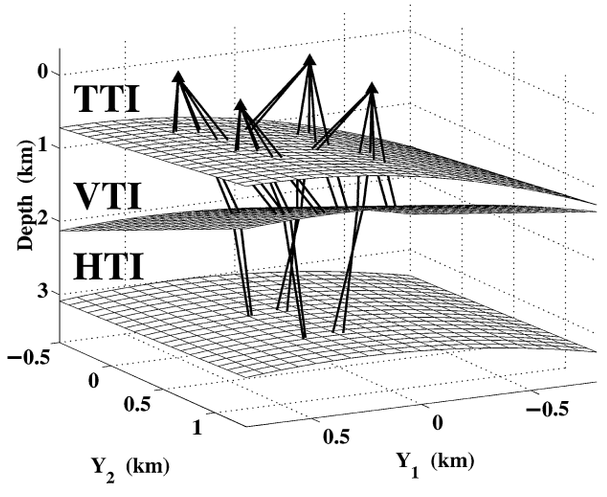

FIG. 8. Zero-offset rays of the PP- and SS(SV SV)-waves for a model composed of TTI, VTI, and HTI layers.

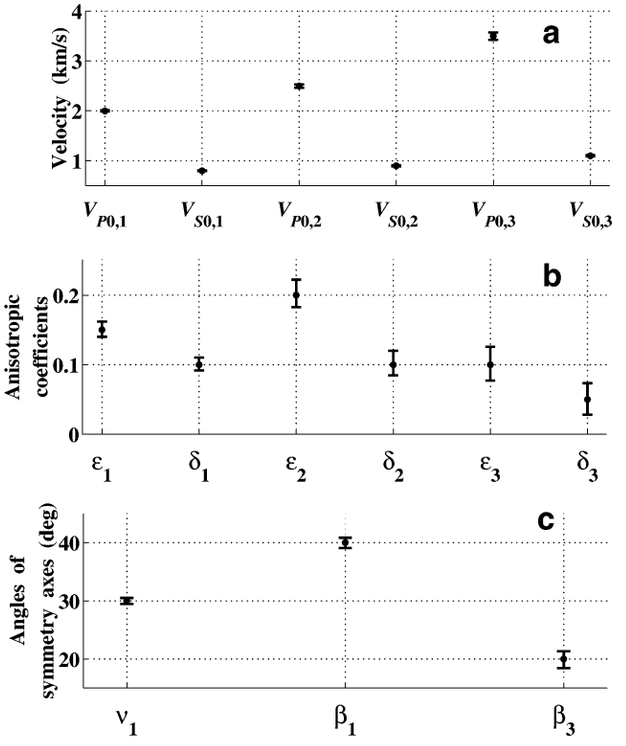

FIG. 9. Results of stacking-velocity tomography for the model in Figure 8. The parameters ν_1 and β_1 are the tilt and azimuth of the symmetry axis in the top (TTI) layer; β_3 is the symmetry-axis azimuth in the bottom (HTI) layer.

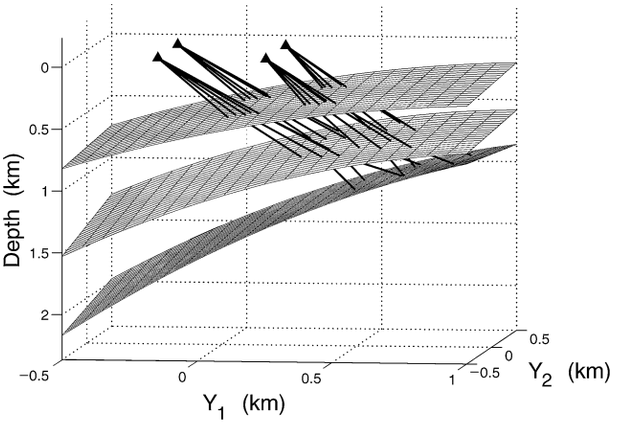

FIG. 10. Zero-offset rays of the PP- and SS(SV SV)-waves for a model composed of two VTI layers on top of an HTI layer. The interval parameters are listed in the top row of Table 2.

the subsurface layer using the most shallow PP and PS reflections. Then, fixing the obtained values, we can determine the interval parameters of the second layer by inverting the traveltimes from its bottom, and the parameter-estimation procedure continues downward. In addition to eliminating upward error propagation from the deeper layers, the stripping approach is computationally efficient because only a few unknowns need to be found at each stage (i.e., for each layer). The main shortcoming of layer stripping is its implicit reliance on the assumption that the reflections from the bottom of the layer contain full information about the layer parameters. Since it is not always the case for PP-waves in TI media (Le Stunff et al., 1999; Grechka et al., 2000a,b), one can expect that for some models the layer-stripping method may create ambiguity in the joint inversion of PP and PS data.

In the second test, the top (VTI) layer was assumed to have HTI symmetry. Then, in addition to the expected significant errors for this layer, we also obtained distorted parameters in both bottom layers (see the third row in Table 2). This test underscores the importance of choosing the right type of anisotropy in the overburden because any errors in the shallow part of the section will propagate through the whole model.

An alternative to assuming a specific type of anisotropy is to adopt the more general tilted TI (or even orthorhombic) model from the outset of the inversion. The correct type of anisotropy can then be identified from the determined orientation of the symmetry axis (for TTI media) or relationships between the estimated anisotropic coefficients (for orthorhombic media). However, according to the above numerical results, the need to estimate the tilt of the symmetry axis often reduces the stability of the algorithm, especially for models close to VTI.

Influence of heterogeneity

Accurate reconstruction of vertical and lateral velocity variations is the main challenge in reflection tomography. For example, even for isotropic media certain types of vertical velocity variations can never be resolved from the reflection traveltimes, no matter how the inversion is performed (e.g., Goldin, 1986). Given the complexity of this problem for anisotropic media, the discussion here is limited to a numerical example illustrating the errors in the estimated anisotropic parameters caused by heterogeneity unaccounted for in the inversion.

Suppose we attempt to estimate the parameters of the VTI overburden for the model from Table 2 (Figure 10) using only the reflections from the second interface. The effective parameters of the overburden then change both vertically (since it actually consists of two layers) and laterally (because the first interface is not horizontal). While the vertical variations of the VTI parameters cannot be resolved without including reflections from the first interface, we can try to estimate the lateral parameter variations by performing the inversion for a range of CMP coordinates Y_1 (Figure 10).

The data $\mathbf{d}(Q, \mathbf{Y}, n)$ [equation (2)] were generated for $Q =$ PP, SV SV, and $n = 2$; the CMP coordinates were varied as $Y_1 = [-0.6, -0.4, \ldots, 0.8, 1.0]$ km, $Y_2 = [-0.2, 0.2]$ km. In each inversion, we used four adjacent CMPs (that form the corners of a rectangle) and assigned the estimated anisotropic coefficients to the center of the rectangle. Treating the overburden as a single homogeneous VTI layer yields the parameters displayed in Figure 11. Clearly, all estimated quantities change

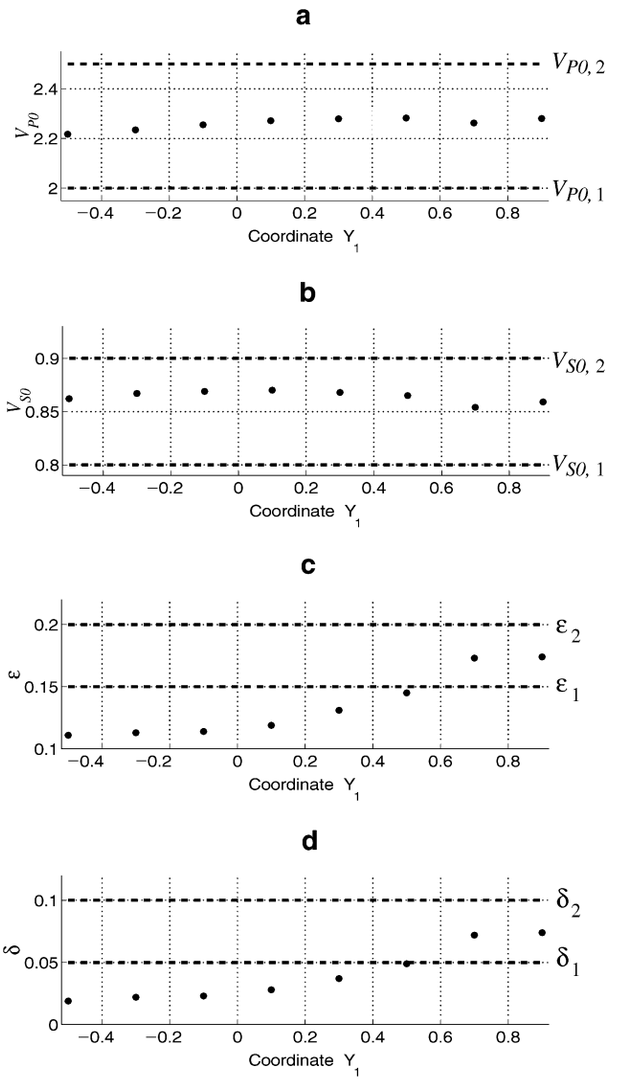

FIG. 11. Effective parameters (dots) of the VTI overburden estimated using the reflections from the second interface in Figure 10. The correct parameters of the VTI layers that make up the overburden are marked by the dashed lines. The coordinate Y_1 (in kilometers) is defined in the text.

Table 2. Correct parameters of the model composed of two VTI layers on top of an HTI layer (top row) and the inversion results based on erroneous assumptions about the symmetry in one of the layers.

	$V_{P0,1}$	$V_{S0,1}$	ϵ_1	δ_1	β_1	$V_{P0,2}$	$V_{S0,2}$	ϵ_2	δ_2	$V_{P0,3}$	$V_{S0,3}$	ϵ_3	δ_3	β_3
Correct model parameters	2.00	0.80	0.15	0.05	–	2.50	0.90	0.20	0.10	3.50	1.10	0.20	0.05	30
Inversion, bottom layer VTI	1.98	0.79	0.16	0.06	–	2.53	0.90	0.18	0.09	3.00	1.28	0.35	0.34	–
Inversion, top layer HTI	2.23	0.94	0.01	0.03	101	2.61	0.92	0.15	0.02	3.55	0.92	0.24	−0.09	34

laterally because the variations in the dip and depth of the interfaces make the overburden laterally heterogeneous. It is interesting that while the effective vertical velocities V_{P0} and V_{S0} (Figure 11a,b) can be regarded as certain averages of the interval velocities, the best-fit anisotropic coefficients ϵ and δ often lie outside the range of the corresponding interval coefficients (Figure 11c,d).

This result, which seems to be puzzling, can be explained by the fact that we operate with a variety of different averages in the stacking-velocity tomography. The "average" or effective parameters produced by the tomographic inversion process are not necessarily bounded by the minimum and maximum interval values. As an example, in the Appendix we show that the effective anisotropic coefficient δ derived from the PP-wave NMO velocity for a stack of plane homogeneous VTI layers can often exceed the maximum interval coefficient δ_n. In the special case of isotropy, when all $\delta_n = 0$, the effective δ above vertically heterogeneous media is always positive (Grechka and Tsvankin, 2003b). The model in Figures 10 and 11 contains curved interfaces, and the averaging procedure is more complicated than that in the Appendix. The results, however, are similar because in both cases the effective values lie outside of the range of the corresponding interval quantities.

In fact, the results in Figure 11 can be considered as a consequence of upscaling, performed implicitly to obtain the effective values of the anisotropic parameters. Replacing the actual heterogeneous medium with the homogeneous model providing the best fit to the data may result in the effective properties which cannot be obtained by the straightforward arithmetic averaging of the corresponding interval (local) properties.

DISCUSSION AND CONCLUSIONS

We introduced a multicomponent tomographic algorithm designed to invert wide-azimuth reflection traveltimes for the interval parameters of TI media. The input data include reflection moveout of PP-waves and converted PS-waves, so the method can be applied in multicomponent ocean-bottom surveys. PS data, however, are not used directly in the velocity-analysis procedure. Instead, they are combined with the PP-wave moveout from the same interface to compute the reflection traveltimes of SS-waves using the model-independent kinematic technique of Grechka and Tsvankin (2002b).

The SS traveltime, in contrast to the more complicated moveout of converted waves, is symmetric with respect to zero offset and (on conventional-length spreads) can be described by the NMO velocity. Azimuthal semblance analysis of PP and SS traveltimes on CMP gathers produces the NMO ellipses and zero-offset traveltimes, which serve as the input to the tomographic inversion.

Although the stacking-velocity tomography of PP and SS data does not use the far-offset information (i.e., nonhyperbolic moveout), it has significant advantages over conventional reflection tomography. The first advantage, which is critically important in anisotropic media, is related to computational efficiency. Since the NMO ellipse (and, therefore, the multiazimuth, multioffset hyperbolic moveout as a whole) can be computed by tracing only one zero-offset ray for each reflection event at a given CMP location, the number of rays to be generated in forward modeling is reduced by orders of magnitude, which makes anisotropic traveltime tomography computationally feasible for complex subsurface models. Second, it is possible to derive semianalytic expressions for the NMO ellipse even in arbitrarily anisotropic media, if the model is structurally simple (Grechka et al., 1999; Grechka and Tsvankin, 1999b, 2002a). Such analytic solutions help to identify the parameters (or the parameter combinations) constrained in the inversion of NMO velocities. Third, restricting the range of source-receiver offsets reduces the influence of lateral heterogeneity on reflection traveltimes, and the velocity field can be estimated separately for blocks of relatively small lateral extent. Within each block, the layers can be treated as homogeneous, and the interfaces can be approximated by simple smooth surfaces, such as low-order polynomials. Then global smoothing can be applied to build the laterally varying anisotropic velocity field and reflecting interfaces.

Here, the multicomponent tomography was implemented for a stack of transversely isotropic layers separated by smooth interfaces. The detailed analysis for a homogeneous TI medium and numerical testing for layered models show that for a range of reflector dips and tilt angles of the symmetry axis, the combination of PP and PSV (or SV SV) data can be used to build anisotropic models for depth processing. The most notable exception is horizontally layered VTI media, where even long-spread (nonhyperbolic) moveout of PP- and PSV-waves does not constrain the vertical velocities (Grechka and Tsvankin, 2003a). In contrast, for HTI media the inversion procedure is quite stable for both horizontal and dipping reflectors. The parameter-estimation results can be compromised by assuming the wrong anisotropic symmetry in one of the layers (e.g., VTI instead of HTI). In principle, such errors can be avoided by using the most general TTI model in the inversion, but the need to estimate the tilt typically reduces the stability of the algorithm.

For a restricted class of models composed of isotropic and VTI layers separated by dipping or irregular interfaces, PP reflection data alone can be used to determine the depth scale of the medium and parameters ϵ and δ (Grechka et al., 2000a,b). This inversion, however, breaks down if the difference $\epsilon - \delta$ is small and the anisotropy is close to elliptical. As follows from our results, combining PP- and PSV-waves resolves this ambiguity (in the presence of reflector dip). Extending the argument of Dellinger and Muir (1988), we can state that since the velocity function of SV-waves in elliptical media is purely isotropic, it does not allow the stretching of the model in the vertical direction that causes the depth uncertainty for PP-waves.

Some common features of geologic formations, such as small-scale velocity heterogeneity, cannot be incorporated into our models because of the limited spatial and amplitude resolution of seismic data. Those features, however, do influence the reflection traveltimes and can significantly alter the values of the estimated parameters. We demonstrated that if heterogeneity is not properly accounted for, the inverted effective parameters providing the best fit to the input data may lie outside the range determined by the corresponding minimum and maximum interval (local) values. Therefore, the anisotropic parameters obtained from the tomographic inversion may bear a significant imprint of the adopted subsurface model.

Successful application of the tomographic algorithm introduced here to a multicomponent data set from the North Sea is discussed in the companion paper by Grechka et al. (2002).

ACKNOWLEDGMENTS

We are grateful to members of the A(nisotropy)-Team of the Center for Wave Phenomena (CWP), Colorado School of Mines, for useful discussions. Suggestions of the associate editor and the reviewers of *Geophysics* helped to improve the manuscript. The support for this work was provided by the members of the Consortium Project on Seismic Inverse Methods for Complex Structures at CWP and by the Chemical Sciences, Geosciences and Biosciences Division, Office of Basic Energy Sciences, U.S. Department of Energy.

REFERENCES

Alkhalifah, T., and Tsvankin, I., 1995, Velocity analysis for transversely isotropic media: Geophysics, **60**, 1550–1566.
Alkhalifah, T., Tsvankin, I., Larner, K., and Toldi, J., 1996, Velocity analysis and imaging in transversely isotropic media: Methodology and a case study: The Leading Edge, **15**, No. 5, 371–378.
Contreras, P., Grechka, V., and Tsvankin, I., 1999, Moveout inversion of *P*-wave data for horizontal transverse isotropy: Geophysics, **64**, 1219–1229.
Dellinger, J., and Muir, F., 1988, Imaging reflections in elliptically anisotropic media: Geophysics, **53**, 1616–1618.
Dix, C. H., 1955, Seismic velocities from surface measurements: Geophysics, **20**, 68–86.
Goldin, S. V., 1986, Seismic traveltime inversion: Soc. Expl. Geophys.
Granli, J. R., Arntsen, B., Sollid, A., and Hilde, E., 1999, Imaging through gas-filled sediments using marine shear-wave data: Geophysics, **64**, 668–677.
Grechka, V., and Tsvankin, I., 1998, 3-D description of normal moveout in anisotropic inhomogeneous media: Geophysics, **63**, 1079–1092.
——— 1999a, 3-D moveout inversion in azimuthally anisotropic media with lateral velocity variation: Theory and a case study: Geophysics, **64**, 1202–1218.
——— 1999b, 3-D moveout velocity analysis and parameter estimation for orthorhombic media: Geophysics, **64**, 820–837.
——— 2000, Inversion of azimuthally dependent NMO velocity in transversely isotropic media with a tilted axis of symmetry: Geophysics, **65**, 232–246.
——— 2002a, NMO-velocity surfaces and Dix-type formulas in anisotropic heterogeneous media: Geophysics, **67**, 939–951.
——— 2002b, PP + PS = SS: Geophysics, **67**, in press.
——— 2003a, On the joint nonhyperbolic moveout inversion of PP and PS data in VTI media: Geophysics, in press.
——— 2003b, Processing-induced anisotropy: Geophysics, in press.
Grechka, V., Pech, A., and Tsvankin, I., 2000a, Inversion of *P*-wave data in laterally heterogeneous VTI media, part I: Plane dipping interfaces: 70th Ann. Internat. Mtg., Soc. Expl. Geophys., Expanded Abstracts, 2225–2228.
——— 2000b, Inversion of *P*-wave data in laterally heterogeneous VTI media, part II: Irregular interfaces: 70th Ann. Internat. Mtg., Soc. Expl. Geophys., Expanded Abstracts, 2229–2232.
Grechka, V., Tsvankin, I., Bakulin, A., Hansen, J. O., and Signer, C., 2002, Joint inversion of PP and PS reflection data for VTI media: A North Sea case study: Geophysics, **67**, 1382–1395, this issue.
Grechka, V., Tsvankin, I., and Cohen, J. K., 1999, Generalized Dix equation and analytic treatment of normal-moveout velocity for anisotropic media: Geophys. Prosp., **47**, 117–148.
Le Stunff, Y., and Grenié, D., 1998, Taking into account a priori information in 3D tomography: 68th Ann. Internat. Mtg., Soc. Expl. Geophys., Expanded Abstracts, 1875–1878.
Le Stunff, Y., Grechka, V., and Tsvankin, I., 2001, Depth-domain velocity analysis in VTI media using surface *P*-wave data: Is it feasible? Geophysics, **66**, 894–903.
Nolte, B., Bishop, K., and Sukup, D., 1999, Anisotropic prestack depth migration of converted-wave data from the Gulf of Mexico: 69th Ann. Internat. Mtg., Soc. Expl. Geophys., Expanded Abstracts, 691–694.
Pérez, M. A., Grechka, V., and Michelena, R. J., 1999, Fracture detection in a carbonate reservoir using a variety of seismic methods: Geophysics, **64**, 1266–1276.
Thomsen, L., 1986, Weak elastic anisotropy: Geophysics, **51**, 1954–1966.
——— 1999, Converted-wave reflection seismology over inhomogeneous, anisotropic media: Geophysics, **64**, 678–690.
Tsvankin, I., 1997, Reflection moveout and parameter estimation for horizontal transverse isotropy: Geophysics, **62**, 614–629.
——— 2001, Seismic signatures and analysis of reflection data in anisotropic media: Elsevier Science Publ. Co., Inc.
Tsvankin, I., and Grechka, V., 2000a, Dip moveout of converted waves and parameter estimation in transversely isotropic media: Geophys. Prosp., **48**, 257–292.
——— 2000b, Two approaches to anisotropic velocity analysis of converted waves: 70th Ann. Internat. Mtg., Soc. Expl. Geophys., Expanded Abstracts, 1193–1196.
Vernik, L., and Liu, X., 1997, Velocity anisotropy in shales: A petrophysical study: Geophysics, **62**, 521–532.

APPENDIX

EFFECTIVE PARAMETER δ FOR LAYERED VTI MEDIA

As an example of the relationship between the effective and interval anisotropic parameters, consider the effective P-wave NMO velocity $\langle V_{\mathrm{nmo},P}\rangle$ for a stack of horizontal homogeneous VTI layers. (Here $\langle a\rangle$ denotes the effective value of the parameter a.) The effective value $\langle V_{\mathrm{nmo},P}\rangle$ can be found using the Dix (1955) averaging of the interval NMO velocities

$$\langle\tau\rangle\langle V_{\mathrm{nmo},P}\rangle^2 = \sum_n \tau_n V^2_{\mathrm{nmo},P,n}, \tag{A-1}$$

where τ_n are the interval one-way zero-offset traveltimes, $V_{\mathrm{nmo},P,n}$ are the interval zero-dip NMO velocities, and

$$\langle\tau\rangle = \sum_n \tau_n \tag{A-2}$$

is the total (effective) zero-offset traveltime. $V_{\mathrm{nmo},P,n}$ are expressed through the interval vertical velocities $V_{P0,n}$ and anisotropic coefficients δ_n in equation (4):

$$V^2_{\mathrm{nmo},P,n} = V^2_{P0,n}(1+2\,\delta_n). \tag{A-3}$$

The products of the interval vertical velocities $V_{P0,n}$ and zero-offset traveltimes τ_n yield the layer thicknesses

$$h_n = V_{P0,n}\tau_n. \tag{A-4}$$

The effective vertical velocity can be written as

$$\langle V_{P0}\rangle = \frac{\langle h\rangle}{\langle\tau\rangle} = \frac{\sum_n h_n}{\sum_n \tau_n}. \tag{A-5}$$

Using equations (A-4) and (A-5), we find

$$\left[\frac{1}{\langle V_{P0}\rangle}\right]^{-1} = \langle V_{P0}\rangle = \frac{\langle h\rangle}{\langle\tau\rangle} = \frac{\langle h\rangle}{\sum_n \frac{h_n}{V_{P0,n}}} = \left[\frac{1}{\langle h\rangle}\sum_n \frac{h_n}{V_{P0,n}}\right]^{-1}. \tag{A-6}$$

Equation (A-6) shows that the effective vertical velocity $\langle V_{P0}\rangle$ is the harmonic average of the interval vertical velocities $V_{P0,n}$.

Next, we introduce the effective anisotropic coefficient $\langle\delta\rangle$ defined as in equation (A-3),

$$\langle V_{\mathrm{nmo},P}\rangle^2 = \langle V_{P0}\rangle^2(1+2\langle\delta\rangle). \tag{A-7}$$

Our goal is to find the relationship between the effective $\langle\delta\rangle$ and the interval coefficients δ_n. Substituting equations (A-3), (A-4), (A-5), and (A-7) into the Dix formula (A-1) leads to

$$\langle V_{P0}\rangle(1+2\langle\delta\rangle) = \frac{1}{\langle h\rangle}\sum_n h_n V_{P0,n}(1+2\,\delta_n), \tag{A-8}$$

or

$$1+2\langle\delta\rangle = \frac{\dfrac{1}{\langle h\rangle}\displaystyle\sum_n h_n V_{P0,n}}{\langle V_{P0}\rangle} + 2\frac{\dfrac{1}{\langle h\rangle}\displaystyle\sum_n h_n V_{P0,n}\,\delta_n}{\langle V_{P0}\rangle}. \tag{A-9}$$

Note that equation (A-9) is exact. The first term on the right-hand side is the ratio of the arithmetic and harmonic averages of the vertical velocities, which is always greater than or equal to unity. Therefore, $\langle\delta\rangle$ satisfies the following inequality:

$$\langle\delta\rangle \ge \frac{\dfrac{1}{\langle h\rangle}\displaystyle\sum_n h_n V_{P0,n}\,\delta_n}{\langle V_{P0}\rangle}. \tag{A-10}$$

In particular, if δ_n is constant throughout the section,

$$\delta_1 = \delta_2 = \cdots = \delta_n = \cdots = \tilde{\delta}, \tag{A-11}$$

then inequality (A-10) yields

$$\langle\delta\rangle \ge \tilde{\delta}. \tag{A-12}$$

The equality $\langle\delta\rangle = \tilde{\delta}$ is reached only if the interval velocities $V_{P0,n}$ are equal, which means that the stack of the layers degenerates into a homogeneous medium. Hence, the effective $\langle\delta\rangle$ overestimates the interval values of this parameter.

In the special case of isotropy ($\tilde{\delta} = 0$),

$$\langle\delta\rangle \ge 0. \tag{A-13}$$

According to inequality (A-10), isotropic layering creates an effective VTI medium with a positive parameter δ. For a more detailed discussion of this model, see Grechka and Tsvankin (2003b).

The results of this appendix may help to explain the well-known discrepancy between the laboratory measurements on shale cores, which give both positive and negative values of δ (Thomsen, 1986; Vernik and Liu, 1997), and predominantly positive δ values obtained from surface seismic measurements (e.g., Alkhalifah et al., 1996).

Two VTI layers

Here, we present estimates of the effective parameter $\langle\delta\rangle$ for a simple model composed of two horizontal VTI layers with equal thicknesses $h_1 = h_2$. In this case, equation (A-9) reduces to

$$1+2\langle\delta\rangle = \frac{V_{P0,1}+V_{P0,2}}{4V_{P0,1}V_{P0,2}}[V_{P0,1}+V_{P0,2} + 2(V_{P0,1}\delta_1 + V_{P0,2}\delta_2)]. \tag{A-14}$$

Introducing the ratio of the vertical velocities

$$\upsilon = \frac{V_{P0,2}}{V_{P0,1}}, \tag{A-15}$$

we rewrite equation (A-14) as

$$1+2\langle\delta\rangle = \frac{1+\upsilon}{4\upsilon}[1+\upsilon+2(\delta_1+\upsilon\delta_2)]. \tag{A-16}$$

Equation (A-16) allows us to express the effective $\langle\delta\rangle$ through the velocity ratio υ:

$$\langle\delta\rangle = \frac{(1-\upsilon)^2}{8\upsilon} + \frac{1+\upsilon}{4\upsilon}(\delta_1+\upsilon\delta_2). \tag{A-17}$$

For positive υ, the function $\langle\delta\rangle(\upsilon)$ from equation (A-17) has the only minimum at

$$\upsilon = \sqrt{\frac{1+2\,\delta_1}{1+2\,\delta_2}}. \tag{A-18}$$

The asymptotic values of $\langle\delta\rangle(\upsilon)$ are given by

$$\lim_{\upsilon\to 0}\langle\delta\rangle(\upsilon) = \infty \quad \text{and} \quad \lim_{\upsilon\to\infty}\langle\delta\rangle(\upsilon) = \infty. \tag{A-19}$$

Therefore, for large velocity contrast between the two layers, the effective parameter $\langle\delta\rangle$ significantly exceeds both interval values [$\langle\delta\rangle > \max(\delta_1, \delta_2)$].

This analysis is confirmed by the numerical example in Figure A-1, which shows that the values of $\langle\delta\rangle$ are bounded by the interval parameters δ_1 and δ_2 only for moderate velocity variations when υ does not deviate from unity by more than ± 0.4. For the velocity ratio $\upsilon = 0.5$, $\langle\delta\rangle \approx 0.14$, which is much larger than the maximum interval $\delta = 0.1$.

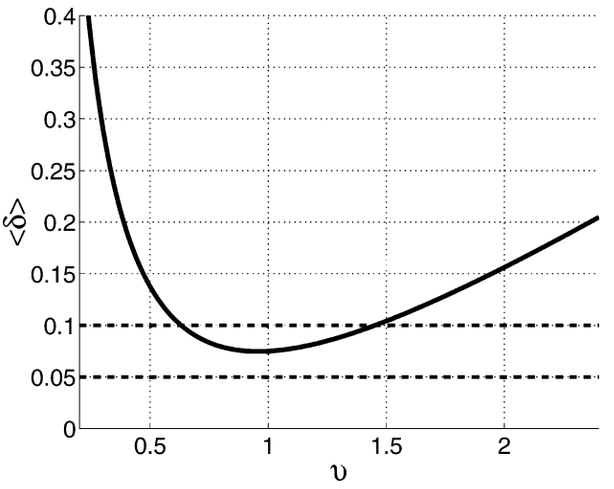

FIG. A-1. The function $\langle\delta(\upsilon)\rangle$ for two horizontal VTI layers (solid). The dashed lines mark the interval anisotropic coefficients $\delta_1 = 0.05$ and $\delta_2 = 0.1$.